Excitatory cholecystokinin neurons of the midbrain integrate diverse temporal responses and drive auditory thalamic subdomains

Lauren J. Kreeger[a,1], Catherine J. Connelly[a], Preeti Mehta[a], Boris V. Zemelman[a], and Nace L. Golding[a,2]

[a]Department of Neuroscience and Center for Learning and Memory, The University of Texas at Austin, Austin, TX 78712-0248

Edited by Dan H. Sanes, New York University, New York, NY, and accepted by Editorial Board Member J. Anthony Movshon January 22, 2021 (received for review July 14, 2020)

The central nucleus of the inferior colliculus (ICC) integrates information about different features of sound and then distributes this information to thalamocortical circuits. However, the lack of clear definitions of circuit elements in the ICC has limited our understanding of the nature of these circuit transformations. Here, we combine virus-based genetic access with electrophysiological and optogenetic approaches to identify a large family of excitatory, cholecystokinin-expressing thalamic projection neurons in the ICC of the Mongolian gerbil. We show that these neurons form a distinct cell type, displaying uniform morphology and intrinsic firing features, and provide powerful, spatially restricted excitation exclusively to the ventral auditory thalamus. In vivo, these neurons consistently exhibit V-shaped receptive field properties but strikingly diverse temporal responses to sound. Our results indicate that temporal response diversity is maintained within this population of otherwise uniform cells in the ICC and then relayed to cortex through spatially restricted thalamic subdomains.

AAV | inferior colliculus | medial geniculate | driver synapses | cholecystokinin

Before reaching the central nucleus of the inferior colliculus (ICC), auditory information is divided into parallel pathways that extract discrete acoustic features, including loudness, spectral information, and localization cues. Parallel inputs recombine in the ICC, which sends information via the ascending tectothalamic pathway to the primary auditory thalamus (ventral division of the medial geniculate body, vMGB) en route to the cortex. Despite their critical position at the nexus between the brainstem and the forebrain, the role of tectothalamic ICC neurons in integrating input features remains controversial. The lemniscal tectothalamic input is commonly regarded as a single phenotype, failing to account for the anatomical and physiological diversity of ICC neurons. Furthermore, it is unclear if the functional diversity of the ICC is a reflection of input patterns or a reflection of intrinsic properties.

Many ICC neurons exhibit responses in vivo that closely resemble inputs from brainstem nuclei carrying spatial information (1–4), suggesting that the ICC collects and reroutes previously processed signals. However, in vivo recordings from guinea pig ICC have shown a continuum in the shape of frequency receptive fields, not the discrete categories that would be expected if responses were merely inherited (5). Although the receptive fields of ICC neurons can resemble those of lower nuclei, intracellular recordings revealed that a complex interplay between inhibitory and excitatory inputs to ICC neurons can also create receptive fields de novo (6, 7). These observations suggest that the ICC does not simply reroute inherited information but instead plays a more transformative role.

Morphologically, ICC neurons consist of either cells with disk-shaped dendritic arbors flattened along the plane of the isofrequency laminae, or stellate cells with dendrites running across isofrequency laminae (8–11). However, dendritic morphology appears to correlate little with membrane properties and firing patterns in vitro (12–16) or with in vivo receptive fields (15–17), and it has remained unclear how much intrinsic membrane properties interact with synaptic inputs to shape auditory information.

Here we identify an ICC neuron population that forms the major lemniscal excitatory projection to the MGB. These cholecystokinin (CCK) expressing neurons exhibit homogeneous intrinsic firing patterns and synaptic properties in vitro and V-shaped frequency receptive fields in vivo. However, even within this seemingly uniform population, we observed diverse temporal responses to tones in vivo, likely reflecting complexity in both intrinsic and extrinsic connectivity. Our results are consistent with a view of midbrain processing where individual cell types perform diverse processing tasks but mediate the convergence of this information onto specific target areas.

Results

Excitatory Cholecystokinin-Containing (CCK_E) Neurons Are the Majority Subpopulation of Excitatory ICC Neurons. We found that a significant population of excitatory neurons in the ICC expresses mRNA for CCK (CCK_E). To quantify the fraction of CCK_E neurons vs. the total neuron population and the more restricted glutamatergic neuron population, we used in situ probes to endogenous CCK, VGluT2, and GAD2. We found that CCK_E neurons make up

Significance

Our ability to identify sounds and understand communication signals depends upon our brains' capacity to combine information about diverse sound features, including temporal patterns. The central nucleus of the inferior colliculus (ICC) performs an initial stage of this integration, but a circuit-based understanding of these processes has been hampered by difficulties in separating clearly defined functional cell types. Here we identify and characterize a major excitatory projection neuron of the ICC. These neurons show uniform intrinsic firing patterns and tuning to frequency, but strikingly diverse temporal responses to sound. Our results suggest that diversity in temporal coding is represented even within a single cell class and is likely primarily driven by differences in circuit connectivity.

Author contributions: L.J.K., C.J.C., B.V.Z., and N.L.G. designed research; L.J.K., C.J.C., and P.M. performed research; L.J.K. and C.J.C. analyzed data; and L.J.K., C.J.C., B.V.Z., and N.L.G. wrote the paper.

The authors declare no competing interest.

This article is a PNAS Direct Submission. D.H.S. is a guest editor invited by the Editorial Board.

[1]Present address: Department of Neurobiology, Harvard Medical School, Boston, MA 02115.

[2]To whom correspondence may be addressed. Email: golding@austin.utexas.edu.

This article contains supporting information online at https://www.pnas.org/lookup/suppl/doi:10.1073/pnas.2007724118/-/DCSupplemental.

Published March 3, 2021.

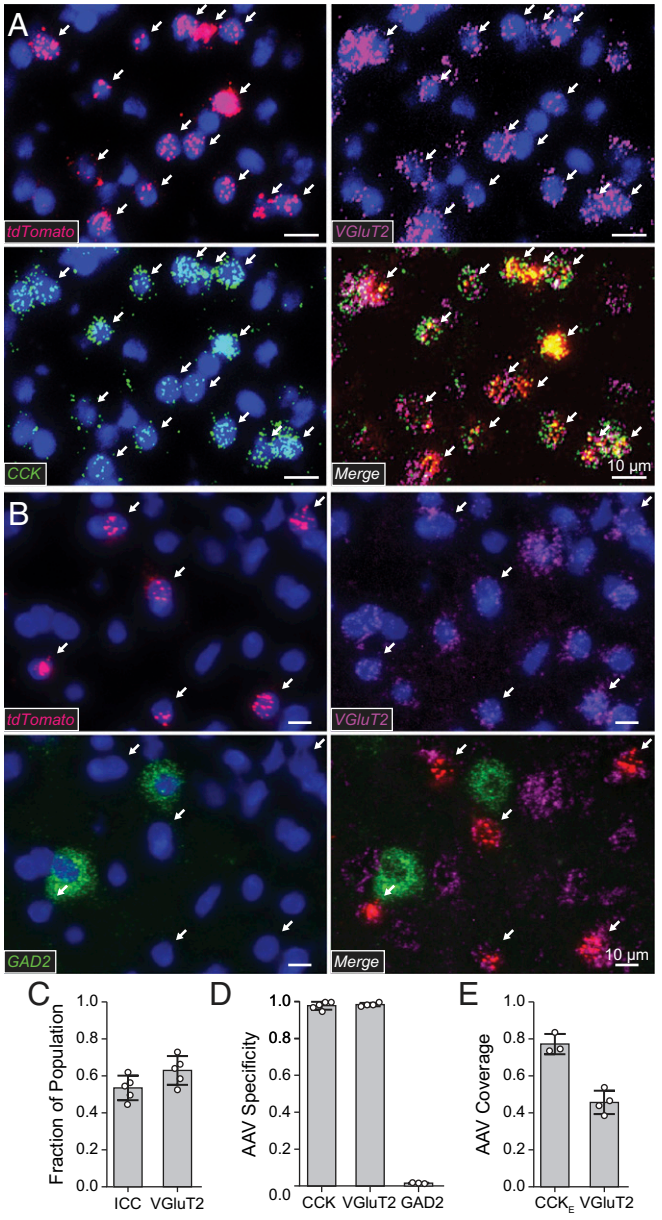

Fig. 1. CCK$_E$ neurons comprise 63% of the excitatory ICC population. Two interdependent AAVs with different promoters were used to target excitatory CCK+ (CCK$_E$) neurons. One vector (AAV:CB3-Flp) expressed Flp recombinase in excitatory and inhibitory CCK neurons. The expression of tdTomato from a second vector was restricted to excitatory neurons and Flp-dependent (AAV:CaMKIIα– (tdTomato)^{Flp}). tdTomato was therefore expressed only in CCK$_E$ neurons. (*A*) Brain sections containing viral-mediated expression of tdTomato were analyzed using in situ mRNA hybridization using probes to tdTomato (red), endogenous VGluT2 (magenta), and endogenous CCK (green) with a DAPI counterstain (blue). Arrows mark CCK$_E$ neurons labeled by virus (CCK+VGluT2+tdTomato+). (*B*) Brain sections containing viral-mediated expression of tdTomato were analyzed using in situ mRNA hybridization using probes to tdTomato (red), endogenous VGluT2 (magenta), and endogenous GAD2 (green) with a DAPI counterstain (blue). Arrows mark CCK$_E$ neurons labeled by virus (VGluT2+tdTomato+GAD2–). (*C*) CCK$_E$ neurons in the ICC express VGluT2 and CCK and comprise a large fraction of the total ICC neuronal population. A total of 53.4 ± 6.6% of ICC neurons are both CCK+ and VGluT2+. A total of 62.9 ± 7.8% of VGluT2+ neurons are CCK+. Open circles indicate measurements from individual gerbils. Bars: mean ± SEM n = 1,220 cells, n = 5 gerbils. (*D*) Nearly all neurons targeted by the viruses were CCK$_E$ neurons. CCK+tdTomato+/tdTomato+, 98.1 ± 2.1%, n = 1,216 cells, n = 5 gerbils; VGluT2+tdTomato+/tdTomato+, 98.7 ± 0.9%, n = 950 cells, n = 4 gerbils; GAD2+tdTomato+/tdTomato+, 2.5 ± 1.5%, n = 432 cells, n = 3 gerbils. (*E*) Targeted neurons represented ~75% of CCK$_E$ neurons and ~50% of VGluT2+ neurons within the 1-mm IC injected site. CCK+tdTomato+VGluT2+/CCK+VGluT2+, 77.4 ± 5.5%, n = 735 cells, n = 3 gerbils; tdTomato+ VGluT2+/VGluT2+, 45.8 ± 6.3%, n = 950 cells, n = 4 gerbils.

53.4 ± 6.6% of the total gerbil ICC population (CCK$_E$/VGluT2) and 62.9 ± 7.8% of the glutamatergic ICC population [CCK$_E$/(VGluT2+GAD2)] (n = 1,220 cells, n = 5 gerbils; Fig. 1*C*).

To target CCK$_E$ neurons specifically, we chose a set intersectional approach (18) using two interdependent adeno-associated virus (AAV) vectors (Fig. 1 *D* and *E*, see *Methods*). Targeted neuron characterization was performed via in situ hybridization and the RNAscope system to evaluate the specificity and coverage of virus-mediated reporter expression in CCK$_E$ neurons (details in *SI Appendix*). Viral-mediated targeting of CCK$_E$ neurons was highly specific, assessed through colocalization of tdTomato mRNA with CCK, VGluT2, and lack of colocalization with GAD2 mRNA (Fig. 1*D*). A total of 98.1 ± 2.1% of neurons positive for tdTomato mRNA were also positive for CCK mRNA (n = 1,216 cells, n = 5 gerbils) and 98.7 ± 0.9% were positive for VGluT2 mRNA (n = 950 cells, n = 4 gerbils). A total of 2.5 ± 1.5% of neurons positive for tdTomato mRNA were also positive for GAD2 mRNA (n = 432 cells, n = 3 gerbils). There was no overlap between GAD2 and VGluT2 mRNA labeling (n = 432 cells, n = 3 gerbils). Viral-mediated expression of tdTomato overlapped a large fraction of CCK$_E$ neurons (Fig. 1*E*). A total of 77.4 ± 5.5% of neurons positive for both CCK and VGlut2 had viral-mediated expression of tdTomato (n = 735 cells, n = 3 gerbils). Furthermore, 45.8 ± 6.3% of VGluT2-containing neurons had viral-mediated expression of tdTomato (n = 950 cells, n = 4 gerbils).

CCK$_E$ Neurons Contribute to the Lemniscal Tectothalamic Pathway. We next investigated the extrinsic targets of CCK$_E$ neurons. Injection of the AAV:CCK$_E$ mixture described above into the ICC (Fig. 2 *A* and *B*) labeled axonal projections with an EGFP reporter later developed in a nickel-diaminobenzadine (Ni-DAB) solution. CCK$_E$ neurons had extensive networks of axon collaterals within the IC. All axons of CCK$_E$ neurons exiting the ICC traversed the brachium of the IC and the vast majority of the terminals were found in the ipsilateral vMGB (Fig. 2*C*). No descending axonal CCK$_E$ projections were seen in the brainstem or external to the tectothalamic pathway, restricting this targeted projection to the primary, or lemniscal, auditory pathway.

CCK$_E$ terminals in the vMGB exhibited large isolated terminal swellings and closely spaced clusters of medium-sized boutons (Fig. 2*D*), which were immunopositive for VGluT2 (*SI Appendix*, Fig. S1). We reconstructed 1,079 CCK$_E$ terminals in two gerbils and quantified maximum diameter (Fig. 2*E*, mean ± SEM: 3.58 ± 0.04 μm, minimum [min]: 1.30 μm, maximum [max]: 8.80 μm), and area (Fig. 2*F*, mean ± SEM: 6.24 ± 0.11 μm^2, min: 0.88 μm^2, max: 26.70 μm^2). Both the axonal projection patterns and terminal morphology of CCK$_E$ neurons are consistent with these cells comprising a major subpopulation of previously described lemniscal tectothalamic drivers (19). Additionally, terminal morphology size and distribution were consistent with previously described Y axons of the retinogeniculate pathway (20).

Finally, for clear visualization of the restricted nature of CCK$_E$ neuron thalamic projection pattern, both CCK$_E$ neurons and all excitatory ICC neurons were labeled in the same viral injection sites with different AAV/reporter constructs (*SI Appendix*, Fig. S2). The broader excitatory population of neurons had prolific descending, intrinsic, commissural, and ascending projections. In stark contrast, CCK$_E$ neurons only projected to the vMGB and appeared to exhibit more topographic specificity relative to the ICC tectothalamic population.

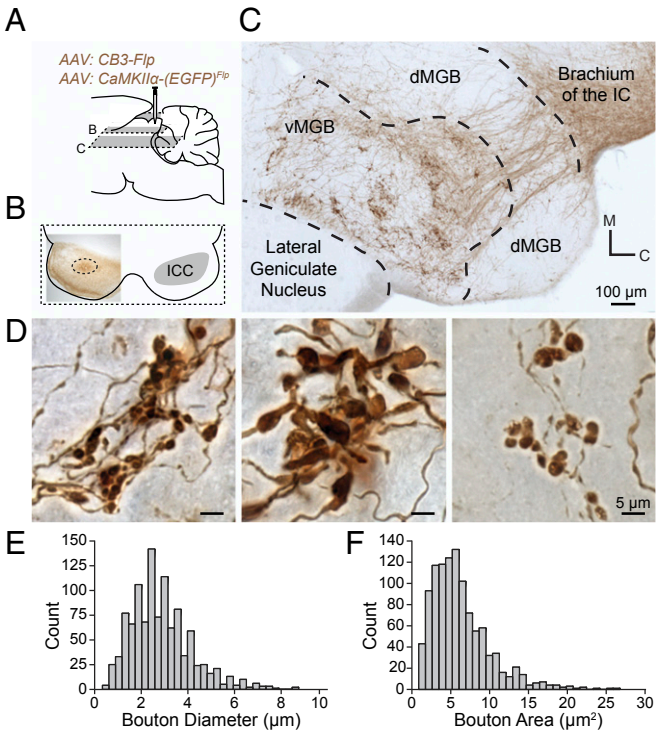

Fig. 2. CCK_E neurons of the ICC have large synaptic terminals in the vMGB. (*A*) A mixture of two AAVs was stereotaxically injected into the ICC to express EGFP in CCK_E neurons. EGFP intensity was enhanced with a biotinylated antibody and visualized with Ni-DAB stain. Gray planes of section denote corresponding locations in *B* and *C*. (*B*) Unilateral ICC injection site (dotted circle) shown in a 65-μm horizontal section. (*C*) A 65-μm horizontal section from the injection in *B*. Axons from CCK_E neurons travel through the brachium of the IC toward the ventral division of the MGB (vMGB). Groups of terminals cluster in the vMGB. (*D*) Representative micrographs demonstrating the diversity of terminal morphology in the vMGB from the injection in *B*. (*E* and *F*) Terminal boutons from CCK_E neurons in the vMGB were reconstructed. Histograms show the distribution of bouton diameter and bouton area (n = 1,079 boutons, n = 2 gerbils).

CCK_E Neurons Are Part of Tectothalamic Driver Circuit. Tectothalamic drivers have been shown to provide powerful excitation to their targets (21–23). To characterize the functional impact of CCK_E synapses onto vMGB neurons, we expressed ChR2 in CCK_E neurons and made whole-cell patch-clamp recordings from vMGB neurons while activating nearby CCK_E axons with short (2 to 3 ms) pulses of blue light (Fig. 3 *A* and *B*). Twenty-one neurons received light-evoked excitatory postsynaptic potentials (EPSPs) from CCK_E axons. Neurons were filled with biocytin and subsequently visualized with streptavidin amplification along with virus-labeled CCK_E axons and terminals (Fig. 3 *C* and *D*).

Light-evoked EPSPs from CCK_E inputs were large enough to reliably produce spikes in 67% (14/21) of vMGB neurons held at a resting potential of −75 mV. On average, the probability of light-evoked spikes at −75 mV was 0.89 ± 0.04. In these cells, trains of light up to and exceeding 50 Hz could reliably drive spikes timed to the onset of each light pulse (Fig. 3*E*). EPSPs were less likely to elicit action potentials (APs) at depolarized resting potentials (−65 mV), possibly due to decreased low-voltage-activated calcium channel activation (Fig. 3 *F*, *Center*). For cells that did spike at −65 mV, the probability of light-evoked spikes was 0.90 ± 0.05. In 33% (n = 7/21) of neurons EPSPs did not produce spikes and averaged 4.37 ± 0.70 mV when cells were held at −65 mV (Fig. 3 *F*, *Left*). For experiments where subthreshold EPSPs were required, we depolarized all neurons to −65 mV and decreased light amplitude to reduce the probability of spiking.

Trains of CCK_E-mediated subthreshold EPSPs activated at −65 mV in thalamic neurons exhibited robust short-term depression (Fig. 3*G*), quantified by measuring the paired pulse amplitude ratio (EPSP2/EPSP1). Depression was greater at higher stimulation frequencies (Fig. 3*H*, n = 7 cells, n = 6 gerbils). No light-dependent activity was seen in EGFP-expressing control neurons.

To assess what types of glutamate receptors mediate EPSPs from CCK_E neurons, we stimulated CCK_E-mediated EPSPs with light and then sequentially blocked AMPA and NMDA receptors, respectively, with bath application of 15 μM NBQX and then a mixture of 15 μM NBQX and 50 μM D-AP5. Neurons with responses that included contributions from voltage-gated calcium channels or spikes were excluded. In vMGB neurons, EPSPs from CCK_E inputs had large AMPA- and NMDA-mediated components, but not metabotropic components (Fig. 3*I*, n = 10 cells, n = 9 gerbils). The relative amplitudes of AMPA and NMDA components were computed from the subtraction of control and drug conditions (Fig. 3 *J* and *K*). The peak voltage change in the AMPA component (7.00 ± 1.59 mV) was measured from the subtraction of the control and D-AP5 condition. The peak voltage change in the NMDA component (2.49 ± 0.59 mV) was measured from the subtraction of the D-AP5 and D-AP5 + NBQX condition. Taken together, the electrophysiological properties of CCK_E synapses onto thalamic neurons fit the profile of a thalamic driver circuit: they comprise large glutamatergic endings or clusters of boutons and provide a powerful but depressing excitatory drive to their thalamic targets mediated by both AMPA and NMDA ionotropic receptors.

CCK_E Neurons Are Disk-Shaped Laminar Neurons. Having established the specificity and functional nature of CCK_E projections, we next asked if CCK_E neurons comprise a single morphological group within the ICC. ICC neurons have been previously separated into two well-defined classes based on dendritic orientation relative to the tonotopic lamina (Fig. 4*A*). Disk-shaped neurons have elongated dendrites oriented parallel to the tonotopic lamina while stellate neurons have radiate dendrites that cross the lamina (8, 10). These two morphologically defined neuron classes include subclasses with distinct physiological properties and neurochemical markers (14, 24–26).

To classify the CCK_E neurons within this diverse framework, we sliced the ICC in the horizontal plane. This plane allowed for the most reliable and reproducible visualization and reconstruction of dendrites within large sections of isofrequency lamina (Fig. 4 *A–C*). Polar histograms with 5° bins around the soma center were used to describe the dendritic orientation of CCK_E neurons. The average polar histogram of all reconstructed neurons (Fig. 4*D*) revealed that dendrites of CCK_E neurons are oriented along the rostromedial to caudolateral axis. The shorter average vector radiating caudolaterally from the cell soma center indicates some truncation of the dendritic tree due to the steeper curvature of the ICC isofrequency lamina as it runs toward the lateral edge of the nucleus. Together, qualitative categorization and quantitation of dendritic orientation suggests CCK_E neurons can be classified as disk-shaped neurons, consistent with past descriptions of this morphological cell type (8, 10).

CCK_E Neurons Exhibit Uniform Intrinsic Firing Patterns. To understand whether CCK_E neurons exhibit distinctive in vitro electrophysiological features relative to the total ICC population, we made whole-cell patch-clamp recordings in slices prepared in either the coronal or ICC laminar planes (Fig. 5*A*). To compare intrinsic firing patterns across multiple ICC neuron populations, we recorded from nonvirally targeted ICC neurons representing the total ICC population, as well as the AAV-labeled excitatory,

NEUROSCIENCE

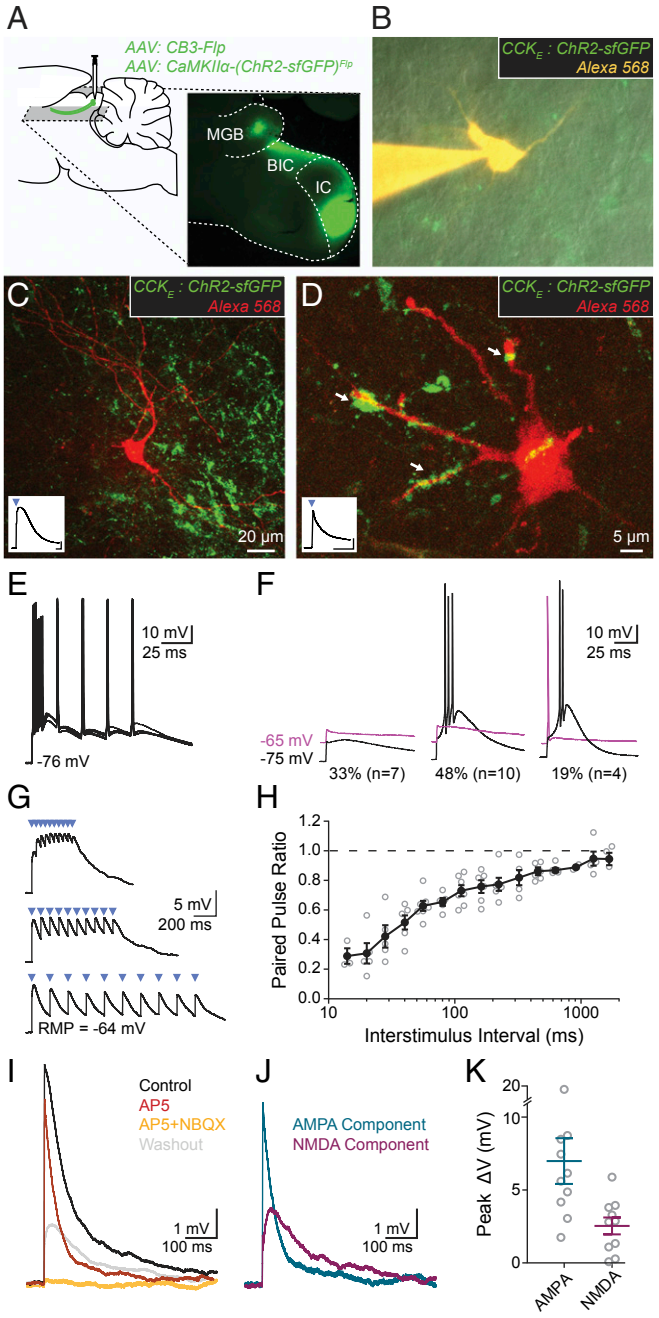

Fig. 3. CCK_E inputs to vMGB neurons mediate large responses through ionotropic synapses exhibiting short-term depression. (*A*) AAV was unilaterally injected into the ICC. Horizontal slices (200 to 250 µm thick) containing the IC and MGB were made for slice physiology experiments. (*B*) vMGB neurons surrounded by axons from CCK_E neurons (green) were targeted for whole-cell patch-clamp recordings and filled with an Alexa dye (orange). (*C* and *D*) Confocal images of recorded vMGB neurons. *Insets* show light-activated EPSPs (2-ms blue light pulse, blue triangle) in the vMGB neuron. EPSP in *C* exhibits widening through activation of low-voltage-activated calcium channels. Axons surrounding neurons with confirmed connections showed diverse terminal sizes and shapes. Arrows in *D* highlight a diversity of putative-synapse sizes. (*Inset* trace scale bars: 1 mV, 20 ms.) (*E*) Light stimulation of CCK_E fibers evoked spikes in 67% (n = 14/21) of vMGB neurons. Spikes were reliable at stimulation rates exceeding 50 Hz. (*F*) 33% of neurons (n = 7/21) had subthreshold light-evoked EPSPs at both hyperpolarized (−75 mV, black) and depolarized (−65 mV, magenta) holding potentials. A total of 48% of neurons (n = 10/21) had light-evoked spikes at hyperpolarized potentials and subthreshold EPSPs at depolarized potentials. The remaining 19% of neurons (n = 4/21) had light-evoked spikes at both hyperpolarized and depolarized holding potentials. (*G*) Trains of light-evoked (blue triangles) CCK_E inputs to vMGB neurons show short-term depression and temporal summation. (*H*) Paired-pulse ratio is plotted as a function of interstimulus interval for vMGB neurons that received light-evoked EPSPs from CCK_E neurons. Closed circles and error bars are mean ± SEM. Open circles correspond to individual neurons. n = 7 neurons, n = 6 gerbils. (*I*) AMPA and NMDA components of EPSPs from CCK_E neurons were pharmacologically isolated using sequential addition of 50 µM D-AP5 (red) and 50 µM D-AP5 + 15 µM NBQX (orange). The D-AP5 + NBQX condition fully blocked all responses. EPSPs were recovered after drug washout (gray). n = 10 neurons, n = 9 gerbils. (*J*) Relative amplitudes of the AMPA and NMDA components were calculated from the subtraction of control and drug conditions. AMPA component (blue): control D-AP5 conditions; NMDA component (magenta): D-AP5–D-AP5/NBQX conditions. (K) EPSPs from CCK_E neurons have large AMPA (7.00 ± 1.59 mV) and NMDA (2.49 ± 0.59 mV) components. Peak voltages were measured from calculated AMPA and NMDA components.

CCK, and CCK_E populations. The data contributing to the total ICC population were not combined with those from animals with virally labeled neurons. However, excitatory, CCK, and CCK_E neurons will have been represented in the population data due to random sampling of unlabeled cells. In both the total ICC and the excitatory populations, we observed the full extent of firing property diversity in the gerbil ICC that has been previously described in other rodents—adapting, sustained, and onset firing patterns (unlabeled ICC: n = 68, 79, and 5/152 neurons, respectively; CaMKIIα: n = 16, 6, and 4/26 neurons, respectively; Fig. 5*B*). CCK neurons exhibited adapting and sustained firing patterns (34 and 5/39 neurons, respectively), but not onset, reflecting a more restricted population of neurons. However, when recordings targeted the CCK_E population, only the adapting firing pattern was observed (n = 35/35 neurons). The rate of adaptation was not a distinguishing property across CCK_E neurons and the general ICC or excitatory cell populations when compared across trains of different rates (Fig. 5*C*). Thus, while firing rate adaption was a consistent feature of CCK_E neurons, it was not unique to this population.

Next we explored if action potential or subthreshold membrane properties would distinguish CCK_E neurons from the less restricted ICC populations. Measures of action potential height and half-width were not distinguishing characteristics between the total, excitatory, and CCK_E populations (Fig. 5*D*). Subthreshold membrane properties were also not distinguishing features of CCK_E neurons (Fig. 5*E*). Taken together, our results show that CCK_E neurons form a uniform neuron population only when intrinsic firing pattern and reporter expression profile are considered together (Fig. 5*B*).

CCK_E Neurons Respond to Sound Stimuli with Diverse Temporal Patterns. To understand the role of CCK_E neurons in conveying auditory information to the thalamus, we measured receptive fields and temporal properties of CCK_E neuron responses to pure tone sound stimuli in vivo. To identify these neurons in vivo, we activated the expressed ChR2 with blue light delivered through an independently placed optic fiber at or just under the dorsal surface of the inferior colliculus (IC) (Fig. 6*A* and *SI Appendix*, Fig. S3; see *Methods*). We recorded the frequency response areas (FRAs) of ICC units (CCK_E: n = 10 units, n = 7 gerbils; total ICC population: n = 61 units, n = 37 gerbils) and divided them into three groups based upon the shape of their excitatory receptive fields in response to contralateral monaural pure tones, as previously described (3). In nontargeted units, we recorded type V units, which had excitatory areas that widened with increasing sound levels; type I units, which had tuning whose shape was insensitive to sound level; and type O units, which displayed an on center-surround receptive field shape. The inhibitory areas for all FRAs were not prominent and spontaneous activity was minimal due to ketamine anesthesia (CCK_E:

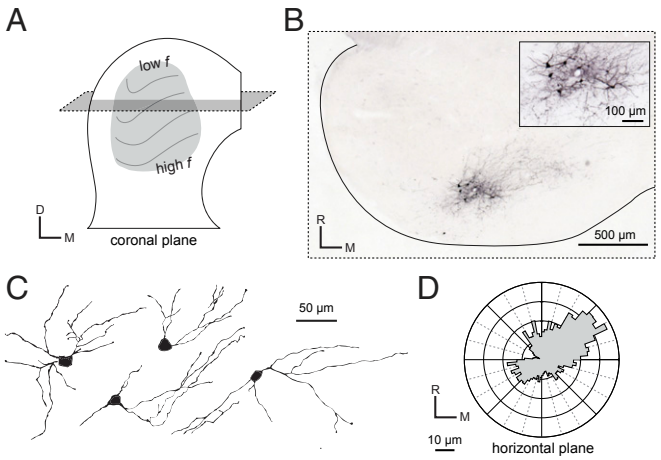

Fig. 4. CCK_E neurons have dendrites oriented along tonotopic lamina. (*A*) The tonotopic organization of the ICC is oriented dorsomedially through paths of fibrodendritic laminae. A horizontal section (gray plane) was used to reconstruct neurons with dendrites along the lamina. (*B*) A representative injection site showing labeled CCK_E neurons with dense axonal arborizations. Slice thickness was 65 μm. To aid detection of fine processes, EGFP intensity was enhanced with a biotinylated antibody and visualized with a Ni-DAB solution. (*C*) Four representative CCK_E neurons along the horizontal plane. (*D*) Average polar plot of reconstructed CCK_E neurons show elongated, disk-shaped dendrites in the horizontal plane. Dendrites tended to be oriented at 45° to the lateral-medial axis.

1.46 ± 2.68 spikes/s; ICC population: 1.92 ± 6.29 spikes/s). In contrast to the nontargeted ICC population, all CCK_E units displayed type V FRAs (Fig. 6*B*, 1 through 4). Q values were calculated to quantify the sharpness of tuning for all receptive fields. CCK_E units typically had wide tuning 20 dB above threshold (Fig. 6*C*). The FRA of one CCK_E V-shaped unit was narrow at its tip as indicated by a large Q_{20}, but the tuning widened by 40 dB above threshold (Fig. 6*D*).

While FRAs to tones of CCK_E neurons were relatively homogeneous, the corresponding temporal responses showed a surprising degree of diversity. Firing patterns in response to 100-ms pure tones at best frequency (BF) were similar to previously described pauser, on-sustained, onset, or sustained ICC responses (16, 27–29). The majority of CCK_E neurons (80% of all CCK_E cells) had temporal responses in which the neuron would fire strongly to the onset of the sound stimuli, followed by a short pause before a second period of robust firing. However, some cells did have an on-sustained or onset-like response to BF tones. Despite the consistency of intrinsic firing types in vitro and FRA shape uniformity in vivo, the diversity in temporal responses in vivo is striking, and most likely reflects the convergence of diverse ascending pathways and potentially intrinsic connections as well.

Discussion

Neurons in brain circuits are typically categorized based on neurotransmitter phenotype, intrinsic electrical properties, dendritic morphology, and network connectivity (30–34). In the ICC, a major center for integrating ascending and descending auditory information, both inhibitory and excitatory cell types share overlapping anatomical and physiological features, underscoring the need to include other information such as molecular-genetic markers. Here, we have combined anatomical and physiological methods with selective virus-based targeting to isolate and define the major excitatory ascending pathway from the ICC to the auditory thalamus. CCK_E neurons of the gerbil ICC have uniform neurochemical, anatomical, and electrophysiological profiles but diverse temporal responses to pure tones. These results support a model of ICC function in which the convergence patterns of inputs, rather than the intrinsic properties of individual cell classes, determines temporal response patterns to sound.

Intersectional Viruses Provide Access to a Family of Excitatory Tectothalamic Neurons. Previous studies of ICC circuit function have described excitatory and inhibitory cell types as having overlapping morphological and physiological characteristics (26, 35, 36). However, using interdependent viral vectors, we have been able to isolate a distinct family of excitatory neurons, comprising ~60% of all excitatory neurons (Fig. 1). These CCK_E neurons have a laminar dendritic orientation and axonal targets specific to neurons of the vMGB. By contrast, nonspecific anatomical tracer studies as well as our own data have shown that axons exiting the ICC diverge to make extensive connections across the auditory system: commissural projections to the contralateral ICC, ascending tectothalamic projections to the MGB, and descending projections to a variety of lower auditory structures (37–39).

CCK_E neurons are distinct from previously identified excitatory neuron subclasses in the ICC. These include regularly firing vasoactive intestinal peptide (VIP)-positive excitatory neurons that display a stellate dendritic morphology and give rise to many ascending and descending projections to both auditory and nonauditory targets (40), and transiently firing excitatory neurons that have low input resistances and express hyperpolarization and cyclic nucleotide-gated ion channels (36). Thus, like inhibitory neurons of the cortex and hippocampus, excitatory neurons of the ICC appear to consist of distinct functional classes whose roles are only beginning to be distinguished. Given the large size of the CCK_E population, it will be important to understand whether this family of neurons can be further parsed into finer subcategories that might carry more restricted kinds of auditory information. These finer subcategories might reflect further intersections with other molecular-genetic markers (33, 41).

CCK_E Neurons Comprise a Powerful Thalamic Driving Circuit in the Auditory Pathway. Using slice optogenetics, we directly demonstrated that activation of CCK_E axons and terminals consistently triggered strong excitatory depolarizations in intracellularly recorded thalamic neurons of the vMGB (Fig. 3). The terminal fields of these afferents did not span the length of a thalamic tonotopic lamina but were instead highly restricted to subdomains (*SI Appendix*, Fig. S2) with tightly clustered large to medium terminal boutons (Fig. 2). Our data are consistent with the driver hypothesis (19), whereby primary ascending lemniscal inputs provide sparse but powerful excitatory drive on the proximal dendrites of thalamic neurons (42, 43). Our observations of small terminal bouton chains that sometimes appeared to target stretches of individual dendrites (e.g., Fig. 3*F*) suggest that large terminal size may not be a prerequisite for strong excitatory drive. Consistent with previous studies of ICC cell types identifying consistent features of ascending driver synapses, CCK_E-mediated synaptic potentials are generated by ionotropic receptors, including a significant NMDA receptor component exhibiting strong short-term depression (21, 23, 44). The magnitude and time course of recovery of short-term depression of optically evoked EPSPs from CCK_E inputs were similar to measurements in studies employing nonselective electrical stimulation of ascending axons (44), indicating that synaptic dynamics of excitatory inputs are conserved across cell classes. The properties of inhibitory synapses also do not distinguish different input classes to ICC neurons (45), further highlighting the fact that ascending pathways in the ICC must be defined jointly by synaptic physiology, intrinsic electrical properties as well as anatomical features.

Tectothalamic afferents of the auditory system and retinothalamic afferents of the visual system share a general anatomical and physiological framework in which parallel inputs carrying sets of highly processed signals provide powerful "driving" input to the thalamus (19). In the visual system, retinal ganglion

NEUROSCIENCE

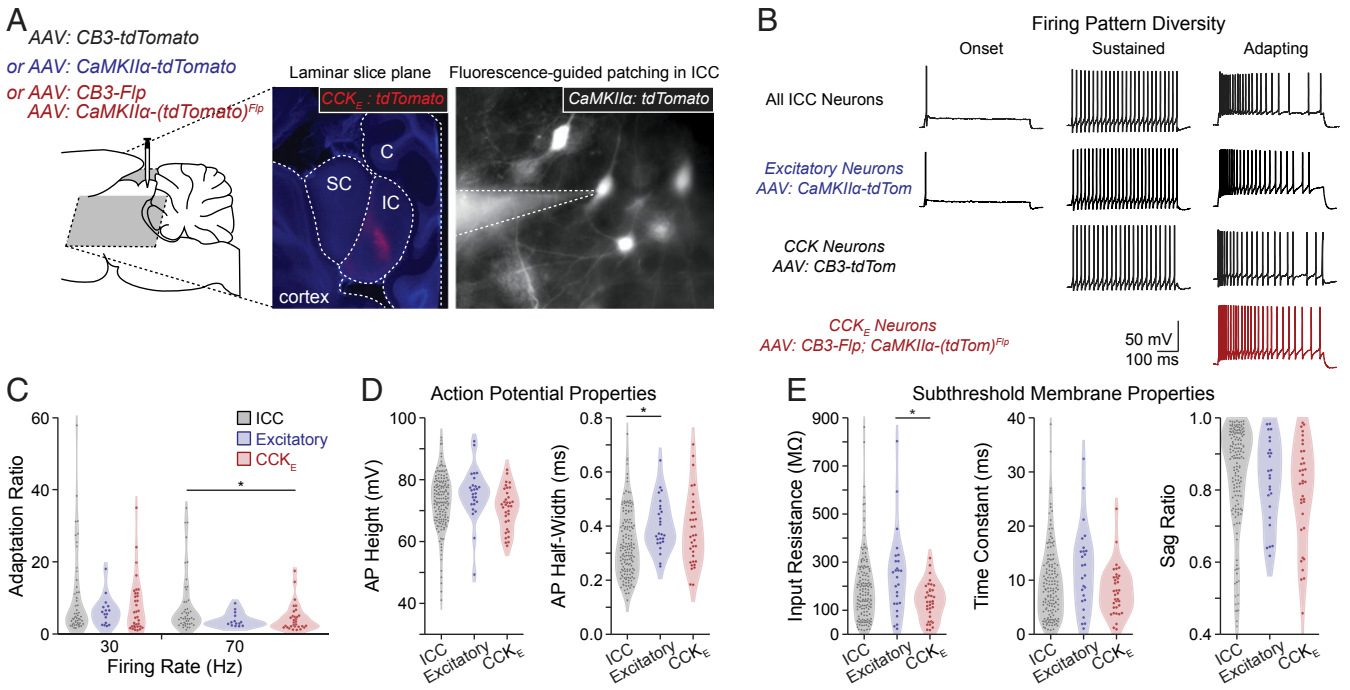

Fig. 5. CCK_E neurons have an adapting firing pattern in vitro. (*A*) AAV injections were made in the gerbil ICC. *Middle* shows a representative slice containing viral targeted CCK_E neurons (red) and counterstained for DAPI after fixation. *Right* shows a recording of a viral targeted excitatory neuron. SC: superior colliculus; IC: inferior colliculus; C: cerebellum. (*B*) Whole-cell current-clamp recordings were made of unlabeled or virus-targeted fluorescent IC neurons. Unlabeled and virus-targeted excitatory neurons displayed the full range of firing pattern diversity, including adapting, sustained, and onset firing patterns (unlabeled: $n = 68$, 79, and 5/152 neurons, respectively, $n = 83$ gerbils; labeled excitatory: $n = 16$, 6, and 4/26 neurons, respectively, $n = 18$ gerbils). Labeled CCK neurons had only adapting and sustained firing patterns (34 and 5/39 neurons, respectively, $n = 18$ gerbils). Labeled CCK_E neurons all had adapting firing patterns ($n = 35/35$ neurons, $n = 21$ gerbils). Sustained and adapting examples had firing rates of ~50 Hz. (*C*) The adapting firing pattern of CCK_E neurons was not different from that of other ICC neurons displaying adapting firing. Adaptation ratios were measured for unlabeled and fluorescence-targeted (all excitatory or CCK_E) neurons for firing rates from bins of 20 to 40 and 60 to 80 Hz. The following are reported as mean ± SEM. Adaptation ratio at 30 Hz: all ICC = 9.9 ± 1.6; all excitatory = 6.3 ± 1.0; CCK_E = 7.7 ± 1.3. Adaptation ratio at 70 Hz: ICC = 8.1 ± 1.2; all excitatory = 3.9 ± 0.5; CCK_E = 4.4 ± 0.7. Sample sizes were ICC: $n = 53$ cells, $n = 41$ gerbils; all excitatory: $n = 16$ neurons, $n = 13$ gerbils; CCK_E: $n = 35$ neurons, $n = 21$ gerbils. ANOVA and subsequent Tukey test resulted in one comparison with $P < 0.05$ (CCK_E and ICC at 70 Hz, $P = 0.043$). (*D* and *E*) Active and subthreshold membrane properties of CCK_E neurons were not different from those of other ICC neurons. Measurements were made from unlabeled and fluorescent excitatory and CCK_E neurons. The following are reported as mean ± SEM. AP height: ICC = 72.95 ± 0.73 mV; all excitatory = 75.45 ± 1.64 mV; CCK_E = 70.78 ± 1.14 mV. AP half-width: ICC = 0.33 ± 0.01 ms; all excitatory = 0.40 ± 0.02 ms; CCK_E = 0.38 ± 0.02 ms. Input resistance: ICC = 195.8 ± 11.7 MΩ, all excitatory = 246.9 ± 34.0 MΩ, CCK_E = 138.0 ± 12.8 MΩ. Time constant: ICC = 9.5 ± 0.5 ms; all excitatory = 12.1 ± 1.5 ms; CCK_E = 8.0 ± 0.8 ms. Sag ratio: ICC = 0.84 ± 0.01; all excitatory = 0.83 ± 0.02; CCK_E = 0.80 ± 0.02. ANOVA and subsequent Tukey test resulted in two comparisons with $P < 0.05$ (AP half-width for ICC and excitatory, $P = 0.014$; input resistance for excitatory and CCK_E, $P = 0.008$).

cells (RGCs) send highly processed information to the visual thalamus (lateral geniculate nucleus) in parallel pathways. Our data for CCK_E terminal morphologies closely match previously reported RGC Y-axon size and termination patterns (20). In mice, RGCs have been classified into at least 25 functionally distinct populations based on molecular, morphological, and physiological criteria, carrying diverse information such as color, temporal pattern, or spatial movement (41, 46–48). In the auditory system, pathways carrying information about horizontal location (time and level difference cues) have been shown to be integrated in different regions of the ICC (49–52), but it is not clear whether these and other cues are carried by distinct neuron populations. The fact that CCK_E neurons are such a large fraction (~60%) of the ICC excitatory neuron population suggests that if subpopulations of neurons exist, carrying specific types of auditory information, they likely will require definition by more than a single marker together with input connectivity, morphology, and electrophysiology.

Functional Implications. In all mammalian species examined, ICC neurons exhibit high diversity in their in vivo spectral tuning with units generally showing V-shaped (most common), I-shaped, and O-shaped FRAs, often in adjacent topographic locations (3, 5, 53). Diversity in the in vivo temporal patterns is also apparent, where ICC units can be described as pauser/build, sustained, regular/sustained, and onset firing groups (16, 27–29). Analyses restricted to neurons with laminar dendritic arbors have also failed to correlate subsets of in vivo responses with dendritic/axonal morphology (17). In vivo recordings of CCK_E neurons revealed V-shaped FRAs, indicating these neurons ascribe similar spectral bandwidth filters to incoming frequency information. By contrast, CCK_E neurons exhibited the full diversity of temporal responses found in the full ICC population (Fig. 6). Such diversity likely reflects differences in how excitatory and inhibitory activity is balanced during acoustic responses (7, 54). Diversity in CCK_E temporal responses may also improve the encoding of both monaural and binaural envelopes that are a hallmark of ICC processing and the salient features of speech and communication signals (55–57).

The striking diversity of subthreshold membrane properties observed in vitro, even within the CCK_E population, likely contributes to the differential filtering properties of ICC neurons in vivo and is consistent with the view that cell types in the ICC convey convergent information from multiple sources. Within each tonotopic ICC lamina, ascending inputs are segregated in

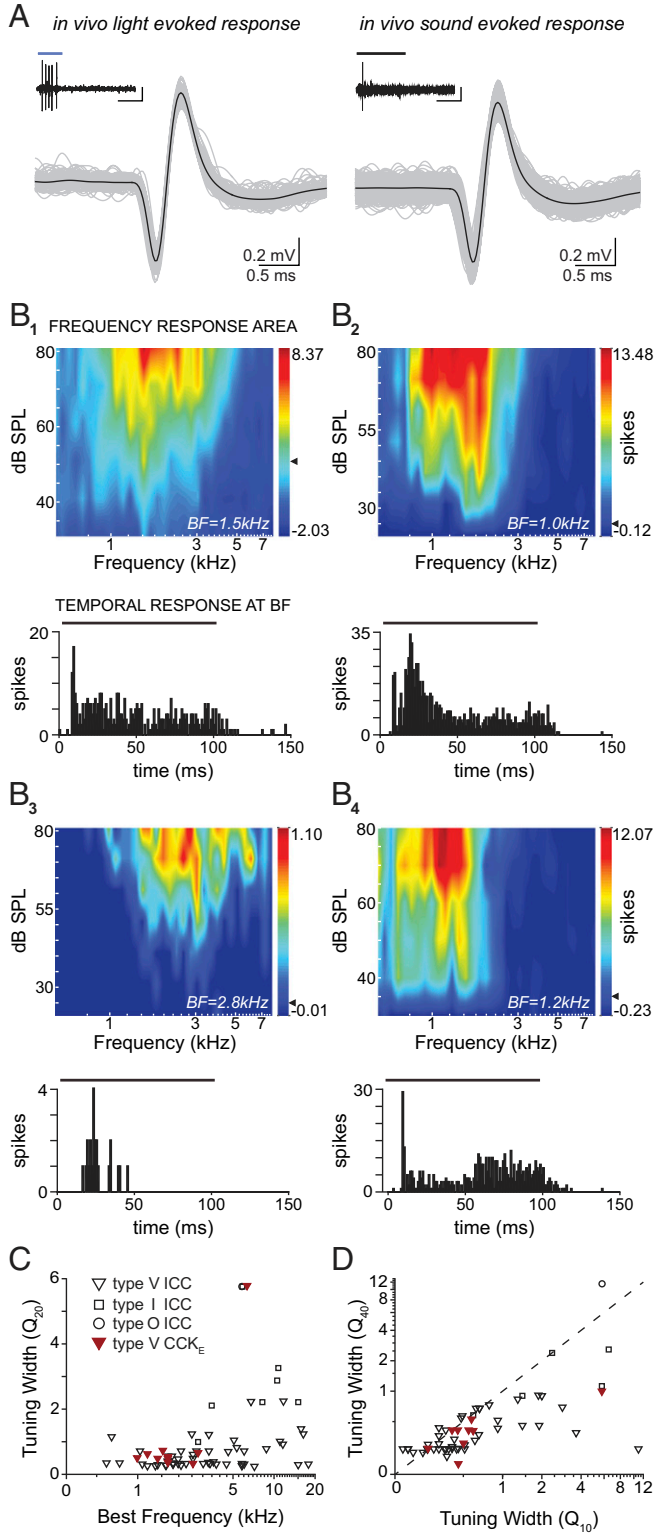

Fig. 6. CCK_E neurons recorded in vivo have uniform V-shaped FRAs and diverse temporal responses to tones. (*A*) Examples of light-evoked (*Left*, 50 ms blue light) and sound-evoked (*Right*, 100 ms 1.5 kHz pure tone at 70 dB sound pressure level [SPL]) voltage traces from one CCK_E unit. Action potentials from light or sound presentations from the respective experiment are aligned and overlaid (gray traces, 103 light-evoked and 1,106 sound-evoked action potentials); black traces, average waveform). *Insets*: Example spike train from one stimulus presentation. (Scale bars: 0.3 mV, 50 ms.) (*B*) Example FRAs from four CCK_E neurons (B1 through 4) and their associated peristimulus time histograms (PSTHs) are shown below each respective FRA. PSTHs were acquired from spike counts (2-ms bin width) at each neuron's best frequency (BF) stimulation at all sound levels tested. The bar above each PSTH indicates tone duration (100 ms). (*C*) Measurements of tuning sharpness as a function of frequency. BF and the FRA Q_{20} values for all recorded units. CCK_E neurons (red) had V-shaped receptive fields. One V-shaped unit was narrower at its tip than others (indicated by a high Q_{20} value) but had a wide low-frequency tail. The sampling of CCK_E neurons was restricted to low and midfrequency regions of the ICC due to limited light penetration and virus injection location. (*D*) Measurements of the shape of FRA curves. Q_{10} is plotted against Q_{40} for each unit. Symbols below the dashed line indicate a widening of the FRA. All FRAs of CCK_E neurons widened with increasing sound level, which is a reflection of their V-shaped tuning.

overlapping functional zones, called synaptic domains, that are targeted by a specific subset of lower auditory nuclei (49–52). CCK_E neurons appear to be distributed evenly across and within tonotopic lamina, and thus neurons within the same and adjacent fibrodendritic laminae likely receive synaptic inputs from different sources, including synapses from ICC collaterals themselves. Given that CCK_E neurons are similar, the unique pattern of inputs each CCK_E neuron receives will result in neurons with different temporal responses to pure tones.

Taken together, the present data indicate that CCK_E neurons are a family of neurons that comprise a large portion of the excitatory tectothalamic driver pathway. These neurons convey temporally diverse auditory information to the vMGB, with temporal response structure determined both by the combination of extrinsic inputs as well as local circuitry. Given its large size, it seems likely that the family of CCK_E neurons may well be divided into subsets of neurons, possibly reflected in characteristic molecular-genetic profiles that will result in further restricted functional properties of these neurons. The intersectional viral approach employed here will be critical to addressing these questions.

Methods

Animal Use. All procedures were approved by and conducted in accordance with The University of Texas at Austin Institutional Animal Care and Use Committee. Male and female Mongolian gerbils (*Meriones unguiculatus*) were bred at the Animal Resource Center at The University of Texas at Austin or obtained from Charles River Laboratories. Gerbils were housed in groups of up to five animals and maintained on a 12 h light/dark cycle.

ICC Neuron Targeting. We restricted targeting to ICC excitatory CCK (CCK_E) neurons using a set intersectional strategy involving two viruses (18). AAV:CB3-Flp and AAV:CaMKIIα-$(XFP)^{Flp}$ ensured that the reporter was expressed only in neurons where both the CB3 and CaMKIIα (58) promoters were active (details in *SI Appendix, Detailed Methods*). The two viruses were combined in a 1:2 vector ratio (recombinase:reporter) based on titer. None of our GABAergic promoters (18) were active in the IC likely due to the developmental origin of IC inhibitory cells (59). To express channelrhodopsin-2 (ChR2) in CCK_E neurons, ChR2(H134R)-sfGFP fusion protein (60) was used in place of fluorescent reporter in the recombinase-dependent vector AAV:CaMKIIα-$(ChR2\text{-}sfGFP)^{Flp}$. Typical titers were 1×10^{10} genomes/microliter.

Histology. For immunohistochemical labeling, tissue was permeabilized and blocked in a solution of 0.2% Triton X-100 and 5% normal goat serum in phosphate-buffered saline. Tissue sections were then incubated with primary antibodies: guinea pig anti-VGluT2 (AB-2251-I, Millipore) and biotinylated goat anti-GFP (ab6658, Abcam) in blocking solution overnight at 4 °C. For fluorescence labeling, sections were incubated with secondary antibody in blocking solution for 2 to 3 h. When using biotinylated antibodies, tissue was incubated in an avidin-biotin solution (Vectastain Elite ABC HRP Kit, Vector Laboratories) and developed in a nickel-diaminobenzadine solution (DAB peroxidase (HRP) Substrate Kit with nickel, Vector Laboratories). Tissue sections were mounted on gelatin-coated slides and coverslipped (Vectashield Hardset Antifade Mounting Medium with DAPI, Vector Laboratories or Permount Mounting Medium, Fisher Scientific).

In thalamic sections developed with Ni-DAB, individual bouton terminals that fell within a cluster of four or more boutons within at least one axonal termination field were traced with Neurolucida software. En passant

boutons corresponding to fibers of passage were not included in the analysis. Divisions of the MGB can be defined immunohistologically with anti-calretinin antibody labeling (1:1,500, CR7697, Swant). Calretinin expresses strongly in the dorsal division of the MGB, but not in the ventral division (61).

We examined the specificity and coverage of virus-mediated reporter expression in CCK_E neurons by multiplexed in situ hybridization using proprietary probes (Advanced Cell Diagnostics) to neuronal marker transcripts: CCK, vesicular glutamate transporter 2 (VGluT2), glutamate decarboxylase 2 (GAD2), and tdTomato reporter. ICC sections were DAPI stained to label nuclei and to aid the colocalization of fluorescence signals (Fig. 1*D*).

Acute Slice Electrophysiology. Data from 230 neurons were obtained from 119 gerbils of both sexes, aged 5 to 8 wk. Gerbils were deeply anesthetized with isoflurane, perfused transcardially with either room temperature or ice-cold artificial cerebral spinal fluid (ACSF; 125 mM NaCl, 25 mM glucose, 25 mM $NaHCO_3$, 2.5 mM KCl, 1.25 mM NaH_2PO_4, 1.5 mM $CaCl_2$, and 1.5 mM $MgSO_4$, pH adjusted to 7.45 with NaOH). Each animal was decapitated, and the brain rapidly removed and submerged in ACSF. For recordings from inferior colliculus neurons ($n = 212$ neurons, $n = 107$ gerbils), 200- to 250-μm slices were prepared in either the coronal or IC laminar plane (45° to horizontal, parallel to IC isofrequency laminae) in room-temperature ACSF. For recordings in the thalamus ($n = 21$ neurons, $n = 12$ gerbils), 200- to 250-μm slices were prepared in the horizontal plane in ice-cold ACSF. Slices were cut with a vibrating microtome (Leica VT1200S; Leica Systems). All preparations were incubated for 30 min at 35 °C, then allowed to recover at room temperature for at least 30 min. ACSF was continuously bubbled with 95% O_2/5% CO_2.

Whole-cell recordings were conducted at 35 °C using a Dagan BVC-700A amplifier (Dagan Corporation) in current-clamp mode using standard methods (*SI Appendix, Detailed Methods*). All membrane potentials are corrected for a 10-mV junction potential. For cell-type-specific fluorescence-targeted or photoactivation recordings, AAV:CB3-Flp and AAV:CaMKIIα-(ChR2-sfGFP)^{FlP} vectors were injected into the inferior colliculus to sensitize CCK_E neurons to light. Full-field 470 nm blue light from a custom LED system was presented through a 20× immersion objective (Zeiss Examiner.D1). Onset, duration, and intensity of LEDs (Luxeon Star) were controlled by a dimmable LED driver (Buckpuck DC driver, Luxeon Star).

In Vivo Surgery and Recordings. Recordings were performed within a sound-attenuation chamber. Forty gerbils aged 11 to 14 wk were anesthetized with an intraperitoneal injection of ketamine hydrochloride (90 mg/kg) and xylazine (18 mg/kg) before being secured to a custom-made head-post holder. Atropine sulfate (0.04 mg/kg) was administered intramuscularly every 30 to 60 min as needed to reduce respiratory mucus secretions. Animals were maintained at 37 °C with a rectal probe feedback low-voltage DC electric heating pad (Harvard Apparatus). Glass-coated tungsten electrodes (2 MΩ) or KCl-filled borosilicate glass electrodes (4 to 10 MΩ) were used for single-unit recordings. For light stimulation, a multimode fiber optic (NA = 0.39, 200 μm core; Thorlabs Inc.) with a polished tip was coupled to an analog modulated blue diode-pumped solid-state laser (λ = 473 nm; Laserglow Technologies) and independently lowered into the craniotomy at 15° off vertical, and ∼2.5 mm below the IC surface.

Stimulus delivery and neural recordings were controlled via custom-made MATLAB software. Acoustic stimuli were generated digitally by an RZ6 Multi I/O Processor (Tucker-Davis Techonologies) and delivered by a calibrated closed-field speaker (ER2; Etymotic Research). Speaker calibration was completed using a 1/2-inch pressure field microphone (4192; Brüel & Kjaer). Neural signals were amplified and filtered (2400B Extracellular Preamplifier; Dagan), before being digitized (RZ6) and sent to the custom software. All sound stimuli were of 100-ms duration and presented at 2/s or 4/s with a 5 ms or 10 ms rise/fall (details for stimuli, histological verification of recording sites, and analyses are included in *SI Appendix, Detailed Methods*).

Data Availability. All study data are included in the article and/or supporting information.

ACKNOWLEDGMENTS. We thank Michael Roberts for his contributions to early stages of the project, and Kenneth Ledford, Stefanie Esmond, and Madeleine H. Flexer Harrison for technical assistance. This work was supported by the NIH (R01 DC006877 to N.L.G., R21DC016169 to N.L.G. and B.V.Z., and U01NS094330 to B.V.Z.). L.J.K. was supported by a graduate research fellowship from the National Science Foundation.

1. K. A. Davis, R. Ramachandran, B. J. May, Single-unit responses in the inferior colliculus of decerebrate cats. II. Sensitivity to interaural level differences. *J. Neurophysiol.* **82**, 164–175 (1999).
2. K. A. Davis, R. Ramachandran, B. J. May, Auditory processing of spectral cues for sound localization in the inferior colliculus. *J. Assoc. Res. Otolaryngol.* **4**, 148–163 (2003).
3. R. Ramachandran, K. A. Davis, B. J. May, Single-unit responses in the inferior colliculus of decerebrate cats. I. Classification based on frequency response maps. *J. Neurophysiol.* **82**, 152–163 (1999).
4. D. McAlpine, D. Jiang, T. M. Shackleton, A. R. Palmer, Convergent input from brainstem coincidence detectors onto delay-sensitive neurons in the inferior colliculus. *J. Neurosci.* **18**, 6026–6039 (1998).
5. A. R. Palmer, T. M. Shackleton, C. J. Sumner, O. Zobay, A. Rees, Classification of frequency response areas in the inferior colliculus reveals continua not discrete classes. *J. Physiol.* **591**, 4003–4025 (2013).
6. S. Kuwada *et al.*, Intracellular recordings in response to monaural and binaural stimulation of neurons in the inferior colliculus of the cat. *J. Neurosci.* **17**, 7565–7581 (1997).
7. N. Li, J. X. Gittelman, G. D. Pollak, Intracellular recordings reveal novel features of neurons that code interaural intensity disparities in the inferior colliculus. *J. Neurosci.* **30**, 14573–14584 (2010).
8. D. L. Oliver, D. K. Morest, The central nucleus of the inferior colliculus in the cat. *J. Comp. Neurol.* **222**, 237–264 (1984).
9. D. L. Oliver, Neuron types in the central nucleus of the inferior colliculus that project to the medial geniculate body. *Neuroscience* **11**, 409–424 (1984).
10. D. L. Oliver, S. Kuwada, T. C. Yin, L. B. Haberly, C. K. Henkel, Dendritic and axonal morphology of HRP-injected neurons in the inferior colliculus of the cat. *J. Comp. Neurol.* **303**, 75–100 (1991).
11. M. S. Malmierca, T. W. Blackstad, K. K. Osen, T. Karagülle, R. L. Molowny, The central nucleus of the inferior colliculus in rat: A Golgi and computer reconstruction study of neuronal and laminar structure. *J. Comp. Neurol.* **333**, 1–27 (1993).
12. Y. Li, M. S. Evans, C. L. Faingold, In vitro electrophysiology of neurons in subnuclei of rat inferior colliculus. *Hear. Res.* **121**, 1–10 (1998).
13. U. Koch, B. Grothe, Hyperpolarization-activated current (Ih) in the inferior colliculus: Distribution and contribution to temporal processing. *J. Neurophysiol.* **90**, 3679–3687 (2003).
14. D. Peruzzi, S. Sivaramakrishnan, D. L. Oliver, Identification of cell types in brain slices of the inferior colliculus. *Neuroscience* **101**, 403–416 (2000).
15. R. Xie, J. X. Gittelman, N. Li, G. D. Pollak, Whole cell recordings of intrinsic properties and sound-evoked responses from the inferior colliculus. *Neuroscience* **154**, 245–256 (2008).
16. M. L. Tan, J. G. Borst, Comparison of responses of neurons in the mouse inferior colliculus to current injections, tones of different durations, and sinusoidal amplitude-modulated tones. *J. Neurophysiol.* **98**, 454–466 (2007).
17. M. N. Wallace, T. M. Shackleton, A. R. Palmer, Morphological and physiological characteristics of laminar cells in the central nucleus of the inferior colliculus. *Front. Neural Circuits* **6**, 55 (2012).
18. P. Mehta *et al.*, Functional access to neuron subclasses in rodent and primate forebrain. *Cell Rep.* **26**, 2818–2832.e8 (2019).
19. S. M. Sherman, R. W. Guillery, Functional organization of thalamocortical relays. *J. Neurophysiol.* **76**, 1367–1395 (1996).
20. M. Sur, M. Esguerra, P. E. Garraghty, M. F. Kritzer, S. M. Sherman, Morphology of physiologically identified retinogeniculate X- and Y-axons in the cat. *J. Neurophysiol.* **58**, 1–32 (1987).
21. E. L. Bartlett, P. H. Smith, Anatomic, intrinsic, and synaptic properties of dorsal and ventral division neurons in rat medial geniculate body. *J. Neurophysiol.* **81**, 1999–2016 (1999).
22. C. C. Lee, S. M. Sherman, Topography and physiology of ascending streams in the auditory tectothalamic pathway. *Proc. Natl. Acad. Sci. U.S.A.* **107**, 372–377 (2010).
23. C. C. Lee, S. M. Sherman, Drivers and modulators in the central auditory pathways. *Front. Neurosci.* **4**, 79 (2010).
24. S. Sivaramakrishnan, D. L. Oliver, Distinct K currents result in physiologically distinct cell types in the inferior colliculus of the rat. *J. Neurosci.* **21**, 2861–2877 (2001).
25. R. Bal, G. G. Green, A. Rees, D. J. Sanders, Firing patterns of inferior colliculus neurons-histology and mechanism to change firing patterns in rat brain slices. *Neurosci. Lett.* **317**, 42–46 (2002).
26. M. Ono, Y. Yanagawa, K. Koyano, GABAergic neurons in inferior colliculus of the GAD67-GFP knock-in mouse: Electrophysiological and morphological properties. *Neurosci. Res.* **51**, 475–492 (2005).
27. A. Rees, A. Sarbaz, M. S. Malmierca, F. E. Le Beau, Regularity of firing of neurons in the inferior colliculus. *J. Neurophysiol.* **77**, 2945–2965 (1997).
28. J. E. Rose, D. D. Greenwood, J. M. Goldberg, J. E. Hind, Some discharge characteristics of single neurons in the inferior colliculus of the cat. I. Tonotopic organization, relation of spike-counts to tone intensity, and firing patterns of single elements. *J. Neurophysiol.* **26**, 321–341 (1963).
29. M. L. Tan, H. P. Theeuwes, L. Feenstra, J. G. Borst, Membrane properties and firing patterns of inferior colliculus neurons: An in vivo patch-clamp study in rodents. *J. Neurophysiol.* **98**, 443–453 (2007).
30. Y. Kawaguchi, Physiological, morphological, and histochemical characterization of three classes of interneurons in rat neostriatum. *J. Neurosci.* **13**, 4908–4923 (1993).
31. T. F. Freund, G. Buzsáki, Interneurons of the hippocampus. *Hippocampus* **6**, 347–470 (1996).

32. D. Battaglia, A. Karagiannis, T. Gallopin, H. W. Gutch, B. Cauli, Beyond the frontiers of neuronal types. *Front. Neural Circuits* **7**, 13 (2013).
33. J. DeFelipe *et al*., New insights into the classification and nomenclature of cortical GABAergic interneurons. *Nat. Rev. Neurosci.* **14**, 202–216 (2013).
34. A. Kepecs, G. Fishell, Interneuron cell types are fit to function. *Nature* **505**, 318–326 (2014).
35. M. Ono, D. C. Bishop, D. L. Oliver, Identified GABAergic and glutamatergic neurons in the mouse inferior colliculus share similar response properties. *J. Neurosci.* **37**, 8952–8964 (2017).
36. V. Naumov, J. Heyd, F. de Arnal, U. Koch, Analysis of excitatory and inhibitory neuron types in the inferior colliculus based on I_h properties. *J. Neurophysiol.* **121**, 2126–2139 (2019).
37. A. Caicedo, H. Herbert, Topography of descending projections from the inferior colliculus to auditory brainstem nuclei in the rat. *J. Comp. Neurol.* **328**, 377–392 (1993).
38. B. R. Schofield, N. B. Cant, Descending auditory pathways: Projections from the inferior colliculus contact superior olivary cells that project bilaterally to the cochlear nuclei. *J. Comp. Neurol.* **409**, 210–223 (1999).
39. A. M. Thompson, G. C. Thompson, Relationship of descending inferior colliculus projections to olivocochlear neurons. *J. Comp. Neurol.* **335**, 402–412 (1993).
40. D. Goyer *et al*., A novel class of inferior colliculus principal neurons labeled in vasoactive intestinal peptide-Cre mice. *eLife* **8**, e43770 (2019).
41. J. R. Sanes, R. H. Masland, The types of retinal ganglion cells: Current status and implications for neuronal classification. *Annu. Rev. Neurosci.* **38**, 221–246 (2015).
42. S. M. Sherman, R. W. Guillery, On the actions that one nerve cell can have on another: Distinguishing "drivers" from "modulators". *Proc. Natl. Acad. Sci. U.S.A.* **95**, 7121–7126 (1998).
43. S. M. Sherman, The thalamus is more than just a relay. *Curr. Opin. Neurobiol.* **17**, 417–422 (2007).
44. E. L. Bartlett, P. H. Smith, Effects of paired-pulse and repetitive stimulation on neurons in the rat medial geniculate body. *Neuroscience* **113**, 957–974 (2002).
45. L. A. Moore, L. O. Trussell, Corelease of inhibitory neurotransmitters in the mouse auditory midbrain. *J. Neurosci.* **37**, 9453–9464 (2017).
46. T. Baden *et al*., The functional diversity of retinal ganglion cells in the mouse. *Nature* **529**, 345–350 (2016).
47. B. G. Cleland, W. R. Levick, H. Wässle, Physiological identification of a morphological class of cat retinal ganglion cells. *J. Physiol.* **248**, 151–171 (1975).
48. H. J. Karten, N. Brecha, Localization of neuroactive substances in the vertebrate retina: Evidence for lamination in the inner plexiform layer. *Vision Res.* **23**, 1197–1205 (1983).
49. D. L. Oliver, M. F. Huerta, "Inferior and superior colliculi" in *Springer Handbook of Auditory Research, Vol. 1, The Mammalian Auditory Pathway: Neuroanatomy*, D. B. Webster, A. N. Popper, R. R. Fay, Eds. (Springer, New York, 1992), pp. 168–221.
50. W. C. Loftus, D. C. Bishop, D. L. Oliver, Differential patterns of inputs create functional zones in central nucleus of inferior colliculus. *J. Neurosci.* **30**, 13396–13408 (2010).
51. D. L. Oliver, Ascending efferent projections of the superior olivary complex. *Microsc. Res. Tech.* **51**, 355–363 (2000).
52. N. B. Cant, Patterns of convergence in the central nucleus of the inferior colliculus of the Mongolian gerbil: Organization of inputs from the superior olivary complex in the low frequency representation. *Front. Neural Circuits* **7**, 29 (2013).
53. C. V. Portfors, Z. M. Mayko, K. Jonson, G. F. Cha, P. D. Roberts, Spatial organization of receptive fields in the auditory midbrain of awake mouse. *Neuroscience* **193**, 429–439 (2011).
54. S. M. Chase, E. D. Young, Limited segregation of different types of sound localization information among classes of units in the inferior colliculus. *J. Neurosci.* **25**, 7575–7585 (2005).
55. R. Batra, S. Kuwada, T. R. Stanford, High-frequency neurons in the inferior colliculus that are sensitive to interaural delays of amplitude-modulated tones: Evidence for dual binaural influences. *J. Neurophysiol.* **70**, 64–80 (1993).
56. L. H. Carney, T. Li, J. M. McDonough, Speech coding in the brain: Representation of vowel formants by midbrain neurons tuned to sound fluctuations. *eNeuro* **2**, ENEURO.0004-15.2015 (2015).
57. M. Dietz, L. Wang, D. Greenberg, D. McAlpine, Sensitivity to interaural time differences conveyed in the stimulus envelope: Estimating inputs of binaural neurons through the temporal analysis of spike trains. *J. Assoc. Res. Otolaryngol.* **17**, 313–330 (2016).
58. T. Dittgen *et al*., Lentivirus-based genetic manipulations of cortical neurons and their optical and electrophysiological monitoring in vivo. *Proc. Natl. Acad. Sci. U.S.A.* **101**, 18206–18211 (2004).
59. L. Lahti, K. Achim, J. Partanen, Molecular regulation of GABAergic neuron differentiation and diversity in the developing midbrain. *Acta Physiol. (Oxf.)* **207**, 616–627 (2013).
60. M. Lovett-Barron *et al*., Regulation of neuronal input transformations by tunable dendritic inhibition. *Nat. Neurosci.* **15**, 423–430, S421-423 (2012).
61. E. Lu, D. A. Llano, S. M. Sherman, Different distributions of calbindin and calretinin immunostaining across the medial and dorsal divisions of the mouse medial geniculate body. *Hear. Res.* **257**, 16–23 (2009).